Journal of Applied Fluid Mechanics, Vol. 9, No. 1, pp. 389-396, 2016.
Available online at www.jafmonline.net, ISSN 1735-3572, EISSN 1735-3645.
DOI: 10.18869/acadpub.jafm.68.224.24158

Numerical Analysis for Peristaltic Motion of MHD Eyring-Prandtl Fluid in an Inclined Symmetric Cannel with Inclined Magnetic Field

F. M. Abbasi [1†], T. Hayat [2, 3] and A. Alsaedi [3]

[1] Department of Mathematics, Comsats Institute of Information Technology, Islamabad 44000, Pakistan
[2] Department of Mathematics, Quaid-I-Azam University 45320, Islamabad 44000, Pakistan
[3] Nonlinear Analysis and Applied Mathematics (NAAM) Research Group, Faculty of Science, King Abdulaziz University, Jeddah 21589, Saudi Arabia

†*Corresponding Author Email: abbasisarkar@gmail.com (F. M. Abbasi)*

(Received October 14, 2014; accepted December 28, 2014)

ABSTRACT

This article addresses the peristaltic transport of Eyring-Prandtl fluid in an inclined asymmetric channel. Heat and mass transfer phenomena along with Soret and Dufour effects is analyzed. Effects of inclined magnetic field and Joule heating are also discussed. Long wavelength approximation is adopted. Numerical computations for flow quantities of interest are analyzed. It is found that the parabolic velocity profile tends to shift from center of the channel towards the channel walls in the case of opposing flow. Velocity and temperature decrease whereas concentration increases by increasing the non-Newtonian parameter. Further the dependence of magnetic field on the angle is quite significant.

Keywords: Peristaltic transport; Inclined magnetic field; Soret and Dufour effects; Joule heating.

1. INTRODUCTION

Fluid transport subject to the sinusoidal waves travelling on the walls of the channel/ tube is termed as peristaltic transport. Motivation about the peristalsis is due to its vast occurring in many physiological mechanisms such as passage of urine from kidney to bladder, spermatozoa transport in the ductus efferentes of the male reproductive tract, blood circulation in the small blood vessels, food stuffs through oesophagus and alimentary canal etc. Utility of such flows persuaded engineers to exploit these in many industrial applications. These include roller finger pumps, heart lung machines and corrosive fluids transport in nuclear industry. It is now well established fact that most of the fluids occurring in physiology and in industry are of non-Newtonian type. Blood, bile, chyme, cosmetic products, mud at low shear rate etc. are examples of non-Newtonian fluids. There are numerous studies available now on the peristaltic motion of viscous and non-Newtonian fluids in a planar channel (see [1-9] and many refs. therein). Little attention has been given to the peristalsis in an inclined channel. For example [10-12].

Simultaneous effects of heat and mass transfer have a key role in processes such as drying, evaporation at the surface of a water body, energy transfer in a wet cooling tower, flow in desert cooler and blood pumps in heart lung machine. Industrial applications of such flows include the methods of generating electric power where electric energy is extracted directly from a moving conducting fluid. Besides this, the knowledge of biomagnetism is useful for diagnostic tests of various clinical disorders which include the utilization of radiations (X-rays, MRI, C.T scan etc.). Radiation therapy for the cure of several diseases (including cancer, removal of blockage in arteries, bleeding reduction in extreme injuries) is a well-known procedure now a days. This makes it worth to study the impact of applied magnetic field on the flows with different flow configurations. Few relevant studies can be seen via attempts [13-21].

The purpose of present communication is to examine the simultaneous effects of heat and mass transfer on the peristaltic transport of Eyring-Prandtl fluid in an inclined asymmetric channel. Inclined magnetic field is considered. In addition Joule heating effect is also included. The flow analysis is modelled and resulting equations are successfully computed. The influence of interesting

variables is explored by graphs and tables.

2. MATHEMATICAL ANALYSIS

Here we consider the flow in an asymmetric channel of width $d_1 + d_2$. The channel is inclined at an angle α. The non-Newtonian fluid is electrically conducting in the presence of an applied magnetic field. The $\bar{X}$ and $\bar{Y}$ axes in Cartesian coordinate system are normal to each other. The channel walls are assumed flexible. Peristaltic waves propagate on the channel walls with constant speed c. The geometries of upper and lower walls are

$$\bar{H}_1(\bar{X},\bar{t}) = d_1 + \varepsilon_1, \text{ upper wall and } \bar{H}_2(\bar{X},\bar{t}) = -(d_2 + \varepsilon_2), \text{ lower wall}$$

where ε_1 and ε_2 are the disturbances produced due to propagation of peristaltic waves at upper and lower walls respectively. These can be taken as follows

$$\varepsilon_1 = a_1 \cos\left(\frac{2\pi}{\lambda}(\bar{X} - c\bar{t})\right),$$

$$\varepsilon_2 = b_1 \cos\left(\frac{2\pi}{\lambda}(\bar{X} - c\bar{t}) + \gamma\right),$$

where a_1, b_1 are the amplitudes of the waves, γ is phase difference and λ is the wavelength. A constant magnetic field of magnitude $\mathbf{B}_0$ making an angle β is incident at the channel, whereas the effects of the induced magnetic field are ignored under the low magnetic Reynolds number assumption. The channel walls are supposed to have temperature and concentration equal to T_0, C_0 (at H_1) and T_1, C_1 (at H_2) respectively. In general the laws of conservation of mass and linear momentum for such a model can be written as

$$\bar{\nabla}\bar{V} = 0,$$

$$\rho\frac{d\bar{V}}{dt} = -\bar{\nabla}\bar{P} + Div\,\bar{\tau} + \bar{J}\times\bar{B} + \rho\bar{g}$$

where $\bar{V} = [U(\bar{X},\bar{Y},\bar{t}), V(\bar{X},\bar{Y},\bar{t}), 0]$ is the velocity field, $\bar{P}$ is the pressure, $\bar{J}$ is the current density, ρ is the density of the fluid, $\bar{g}$ is the gravitational acceleration and $\bar{\tau}$ is the extra stress tensor for the fluid. Here bar indicates the quantities in the fixed frame. These equations along with energy and concentration equations give

$$\bar{U}_{\bar{X}} + \bar{V}_{\bar{Y}} = 0, \tag{1}$$

$$\begin{aligned}\rho\frac{d\bar{U}}{dt} = &-\frac{\partial\bar{P}}{\partial\bar{X}} + \frac{\partial\bar{\tau}_{\bar{X}\bar{X}}}{\partial\bar{X}} + \frac{\partial\bar{\tau}_{\bar{X}\bar{Y}}}{\partial\bar{Y}}\\ &-\sigma B_0^2\cos\beta\left(\bar{U}\cos\beta - \bar{V}\sin\beta\right)\\ &+\rho g\alpha^*\left(T - T_0\right)\sin\alpha\\ &+\rho g\beta^*\left(C - C_0\right)\sin\alpha + \rho g\sin\alpha,\end{aligned} \tag{2}$$

$$\begin{aligned}\rho\frac{d\bar{V}}{dt} = &-\frac{\partial\bar{P}}{\partial\bar{Y}} + \frac{\partial\bar{\tau}_{\bar{Y}\bar{X}}}{\partial\bar{X}} + \frac{\partial\bar{\tau}_{\bar{Y}\bar{Y}}}{\partial\bar{Y}}\\ &-\sigma B_0^2\sin\beta\left(\bar{U}\cos\beta - \bar{V}\sin\beta\right)\\ &-\rho g\alpha^*\left(T - T_0\right)\cos\alpha\\ &-\rho g\beta^*\left(C - C_0\right)\cos\alpha - \rho g\cos\alpha,\end{aligned} \tag{3}$$

$$\begin{aligned}\rho C_p\frac{dT}{dt} = &K\left[\frac{\partial^2 T}{\partial\bar{X}^2} + \frac{\partial^2 T}{\partial\bar{Y}^2}\right] + \bar{\tau}.\bar{L}\\ &+\sigma B_0^2\left(\bar{U}\cos\beta - \bar{V}\sin\beta\right)^2\\ &+\frac{DK_T}{C_s}\left[\frac{\partial^2 C}{\partial\bar{X}^2} + \frac{\partial^2 C}{\partial\bar{Y}^2}\right],\end{aligned} \tag{4}$$

$$\frac{dC}{dt} = D\left[\frac{\partial^2 C}{\partial\bar{X}^2} + \frac{\partial^2 C}{\partial\bar{Y}^2}\right] + \frac{DK_T}{T_m}\left[\frac{\partial^2 T}{\partial\bar{X}^2} + \frac{\partial^2 T}{\partial\bar{Y}^2}\right], \tag{5}$$

in which d/dt is the material derivative, $\bar{\tau}_{ij}$ are the components of the extra stress tensor, $\bar{L}$ the gradient of velocity, α^* he coefficient of thermal expansion, β^* the coefficient of expansion due to concentration, C_p the specific heat, T the temperature, K the thermal conductivity of the fluid, D the mass diffusivity, K_T the thermal diffusion ratio, C_s the concentration susceptibility, σ the electric conductivity and C the concentration.

We transform our problem from fixed to moving frame through the transformations mentioned below [13-14, 20-21]

$$\begin{aligned}&\bar{x} = \bar{X} - c\bar{t},\ \bar{y} = \bar{Y},\ \bar{u} = \bar{U} - c,\\ &\bar{v} = \bar{V},\ \bar{p}(\bar{x},\bar{y}) = \bar{P}(\bar{X},\bar{Y},\bar{t}).\end{aligned} \tag{6}$$

The transformed set of equations may be written as

$$\frac{\partial\bar{u}}{\partial\bar{x}} + \frac{\partial\bar{v}}{\partial\bar{y}} = 0, \tag{7}$$

$$\begin{aligned}&\rho\left(\left(\bar{u}+c\right)\frac{\partial}{\partial\bar{x}} + \bar{v}\frac{\partial}{\partial\bar{y}}\right)\left(\bar{u}+c\right) = -\frac{\partial\bar{p}}{\partial\bar{x}} + \frac{\partial\bar{\tau}_{\bar{x}\bar{x}}}{\partial\bar{x}} + \frac{\partial\bar{\tau}_{\bar{x}\bar{y}}}{\partial\bar{y}}\\ &-\sigma B_0^2\cos\beta\left(\left(\bar{u}+c\right)\cos\beta - \bar{v}\sin\beta\right) + \rho g\alpha^*\left(T - T_0\right)\sin\alpha\\ &+\rho g\beta^*\left(T - T_0\right)\sin\alpha + \rho g\sin\alpha,\end{aligned} \tag{8}$$

$$\begin{aligned}&\rho\left(\left(\bar{u}+c\right)\frac{\partial}{\partial\bar{x}} + \bar{v}\frac{\partial}{\partial\bar{y}}\right)\bar{v} = -\frac{\partial\bar{p}}{\partial\bar{y}} + \frac{\partial\bar{\tau}_{\bar{y}\bar{x}}}{\partial\bar{x}} + \frac{\partial\bar{\tau}_{\bar{y}\bar{y}}}{\partial\bar{y}}\\ &-\sigma B_0^2\sin\beta\left(\left(\bar{u}+c\right)\cos\beta - \bar{v}\sin\beta\right)\\ &-\rho g\alpha^*\left(T - T_0\right)\cos\alpha - \rho g\alpha^*\left(C - C_0\right)\cos\alpha - \rho g\cos\alpha,\end{aligned} \tag{9}$$

$$\rho C_p\left(\left(\bar{u}+c\right)T_{\bar{x}} + \bar{v}T_y\right) =$$

$$K\left[\frac{\partial^2 T}{\partial \bar{X}^2}+\frac{\partial^2 T}{\partial \bar{Y}^2}\right]+\upsilon\left(\bar{\tau}.\bar{l}\right)$$
$$+\sigma B_0^2\left(\left(\bar{u}+c\right)\cos\beta-\bar{v}\sin\beta\right)^2+\frac{DK_T}{C_s}\left[\frac{\partial^2 C}{\partial \bar{X}^2}+\frac{\partial^2 C}{\partial \bar{Y}^2}\right], \tag{10}$$

$$\frac{dC}{dt}=D\left[\frac{\partial^2 C}{\partial \bar{X}^2}+\frac{\partial^2 C}{\partial \bar{Y}^2}\right]+\frac{DK_T}{T_m}\left[\frac{\partial^2 T}{\partial \bar{X}^2}+\frac{\partial^2 T}{\partial \bar{Y}^2}\right]. \tag{11}$$

Here we define the dimensionless quantities as

$$x=\frac{\bar{x}}{\lambda},\ y=\frac{\bar{y}}{d_1},\ u=\frac{\bar{u}}{c},\ v=\frac{\bar{v}}{c\delta},$$
$$\delta=\frac{d_1}{\lambda},\ h_1=\frac{\bar{H}_1}{d_1},$$
$$h_2=\frac{\bar{H}_2}{d_1},\ d=\frac{d_2}{d_1},\ a=\frac{a_1}{d_1},\ b=\frac{b_1}{d_1},$$
$$p=\frac{d_1^2\bar{p}}{c\lambda\eta_0},\ \mathrm{Re}=\frac{\rho c d_1}{\eta_0},$$
$$t=\frac{c\bar{t}}{\lambda},\ \theta=\frac{T-T_0}{T_1-T_0},\ \varphi=\frac{C-C_0}{C_1-C_0},$$
$$\tau=\frac{d_1\tau}{\eta_0 c},Br=\mathrm{Pr}E,$$
$$Fr=\frac{c^2}{gd_1},\ M^2=\left(\frac{\sigma}{\eta_0}\right)B_0^2a^2,$$
$$m=M\cos\beta,\ E=\frac{c^2}{C_p\left(T_1-T_0\right)},$$
$$Du=\frac{D\left(C_1-C_0\right)K_T}{C_s\zeta\eta_0\left(T_1-T_0\right)},\ Sr=\frac{\rho DK_T\left(T_1-T_0\right)}{\eta_0 T_m\left(C_1-C_0\right)},$$
$$Sc=\frac{\eta_0}{\rho D},$$
$$G_t=\frac{\rho g\alpha\left(T_1-T_0\right)d_1^2}{\eta_0 c},\ G_c=\frac{\rho g\alpha^*\left(C_1-C_0\right)d_1^2}{\eta_0 c}$$
$$\mathrm{Pr}=\frac{\eta_0 C_p}{K},$$
$$u=\psi_y,\ v=-\psi_x. \tag{12}$$

Where the continuity equation is identically satisfied, ψ denotes the stream function, υ the kinematic viscosity, Re the Reynolds number, T_m the fluid mean temperature, G_t the local heat Grashoff number, G_c the local mass Grashoff number, Br the Brinkman number, E the Eckret number, Pr the Prandtl number, δ the wave number, η_0 limiting viscosity at zero strain rate, φ dimensionless concentration and the dimensionless temperature is θ.

We seek to analyze the behavior of non-Newtonian fluid namely Eyring-Prandtl fluid model. The corresponding extra stress tensor for this model is [22-23]

$$\bar{\tau}=\left[\frac{A^*\eta_0 arc\,\mathrm{Sin}h\left[\frac{\left|\nabla\bar{V}\right|}{B^*}\right]}{\left|\nabla\bar{V}\right|}\right]\nabla\bar{V}, \tag{13}$$

where A^* and B^* are the material constants for the fluid model. The above equation yields

$$\tau_{xy}=\left\{A-B\left(\psi_{yy}\right)^2\right\}\psi_{yy}. \tag{14}$$

In above equations A and B are the dimensionless forms of the material constants given by

$$A=\frac{A^*}{B^*},\ B=\frac{Ac^2}{3!B^{*2}a^2}.$$

The long wavelength approximation leads to the fact that the half channel width is small compared to the wavelength of peristaltic wave and the low Reynolds number corresponds to the inertia free flow. These considerations are significant for the case of chyme transport through small intestine [1] where half width of the intestine is small in comparison to the wavelength of peristaltic wave. Further, Lew *et al*. [2] concluded that Reynolds number for the fluid mechanics in small intestine is small. Making use of the Eqs. (12) and (14), Eqs. (8-11) under long wavelength and low Reynolds number approximation [13-14, 20-21] yield

$$p_x=\frac{\partial}{\partial y}\left\{A-B\left(\psi_{yy}\right)^2\right\}\psi_{yy}-m^2\left(\psi_y+1\right)$$
$$+G_t\theta\sin\alpha+G_c\theta\sin\alpha+\frac{\mathrm{Re}\sin\alpha}{Fr}, \tag{15}$$

$$p_y=0, \tag{16}$$

$$\theta_{yy}+Br\left\{A\psi_{yy}^2-B\left(\psi_{yy}\right)^4\right\}$$
$$+Brm^2\left(\psi_y+1\right)^2+\mathrm{Pr}Du\left(\varphi_{yy}\right)=0, \tag{17}$$

$$\frac{1}{Sc}\varphi_{yy}+Sr\theta_{yy}=0. \tag{18}$$

It should be noted that the dimensionless form of the equations for the Eyring-Prandtl fluid model can predict the result for the Sutterby fluid model when $A=1$. Only variation is in the value of the parameter B that it is defined in a different way for the Sutterby fluid model. We can recover the equations for viscous fluid when $A=1$ and $B=0$ (in dimensionless form).

Defining ζ and F as the dimensionless mean flows in fixed and moving frames we have

$$\eta=F+1+d \tag{19}$$

where

$$F=\int_{h_2}^{h_1}\frac{\partial\psi}{\partial y}dy. \tag{20}$$

The dimensionless boundary conditions

$$\psi = \frac{F}{2}, \quad \psi_y = -1, \quad \theta = 0, \quad \varphi = 0, \quad at \quad y = h_1,$$
$$\psi = -\frac{F}{2}, \quad \psi_y = -1, \quad \theta = 1, \quad \varphi = 1, \quad at \quad y = h_2, \tag{21}$$

where

$$h_1(x) = 1 + a\cos(2\pi x), \; h_2(x) = -d - b\cos(2\pi x + \gamma), \tag{22}$$

Numerical solutions of the above system subject to the relevant boundary conditions are obtained using Mathematica. In the next section, the obtained results are analyzed.

3. GRAPHICAL ANALYSIS

Here analysis of flow quantities is presented via graphs and Tables. Graphs for the velocity profile, temperature and concentration are plotted in the Figs. 1-3. Numerical values of the heat and mass transfer rates at the wall are given in the Tables 1 and 2. The obtained results are analyzed for both assisting and opposing flows. For assisting flows, the local Grashoff numbers are assigned positive values ($G_t, G_c = +2$) and for opposing flows the values are taken negative ($G_t, G_c = -2$). For the sake of simplicity, throughout the analysis we term the boundary at h_1 as the upper wall and that at h_2 as the lower wall.

Table 1 Heat transfer rate at h 1 for assisting and opposing flows

B	A	M	☹	☺	Assisting flow	Opposing flow
0.0	3.5	1	$\frac{\pi}{4}$	$\frac{\pi}{2}$	0.7029	0.8012
0.08					0.6956	0.7945
0.05	2.5				0.6101	0.7096
	3.5				0.6984	0.7970
		0			0.6715	0.7681
		2			0.7790	1.468
		1	0		0.7253	0.8258
			$\frac{\pi}{2}$		0.6715	0.7681
			$\frac{\pi}{4}$	0	0.7410	0.7410
				$\frac{\pi}{2}$	0.6984	0.7970

Figs. 1 (a-e) are plotted to examine the behavior of velocity profile for change in certain parameters of interest. It is seen through these Figs. that velocity attains maximum value at the center of the channel for both assisting and opposing flows. However, for opposing flow the velocity profile tends to shift towards the upper wall by a considerable amount. Maximum value of the velocity is found to decrease with an increase in B but remains unchanged for an increase in A. However near the channel walls the velocity profile is changed by A, i.e. the velocity decreases near the lower wall when there is an increase in A. Near the upper wall it increases in case of assisting flow. Such behavior of velocity is totally reversed for the case of opposing flow (see Fig. 1 b). Effect of channel inclination on the velocity is examined through Fig. 1 c. Variation in the velocity is observed near the channel walls when inclination angle is increased. Again the behavior of velocity is opposite for the case of assisting and opposing flows. Further it is also seen that the effects of channel inclination is more prominent when the local Grashoff numbers have higher values. Impact of applied magnetic field and its inclination on the velocity is seen through Figs. 1 d and e. Maximum value of velocity is found to decrease with an increase in the value of Hartman number whereas the velocity increases by increasing β. Effects of M and β greatly depend upon each other i.e. change in one quantity effects the behavior of other parameter as well.

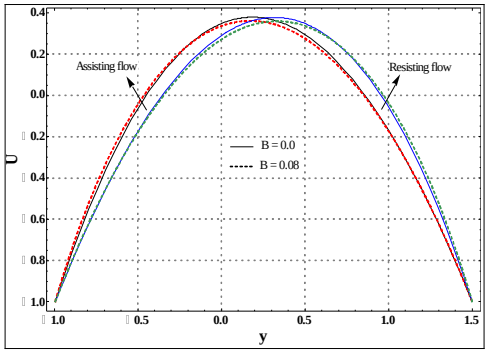

1 (a)

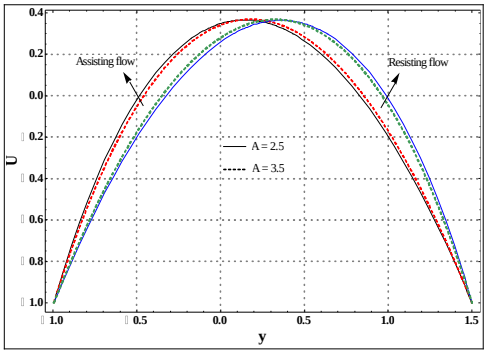

1 (b)

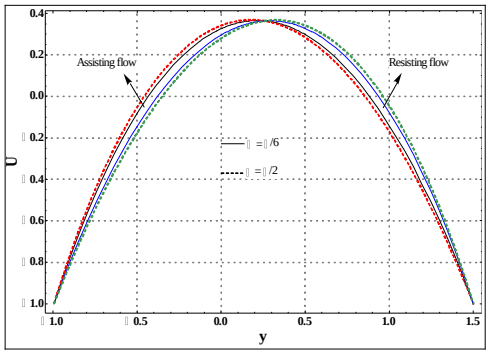

1 (c)

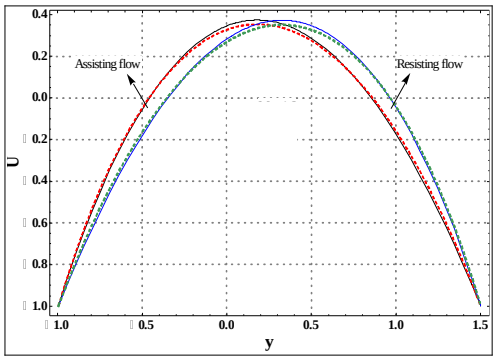

1 (d)

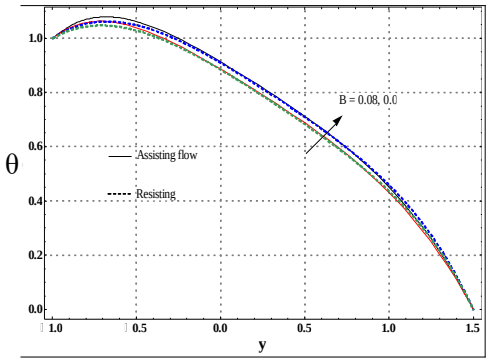

2 (a)

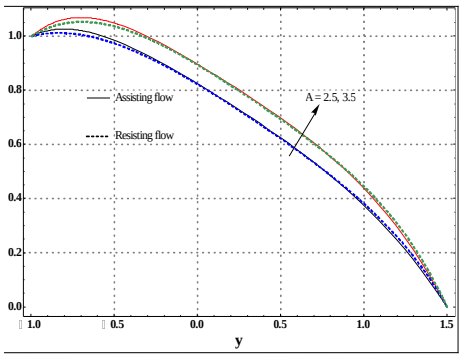

2 (b)

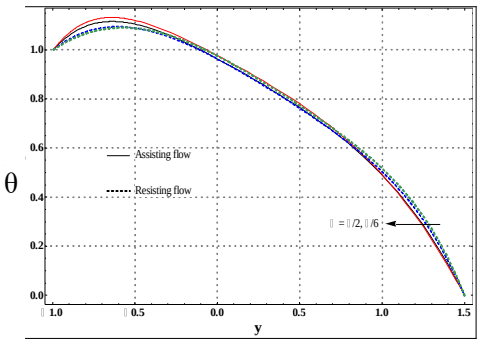

2 (c)

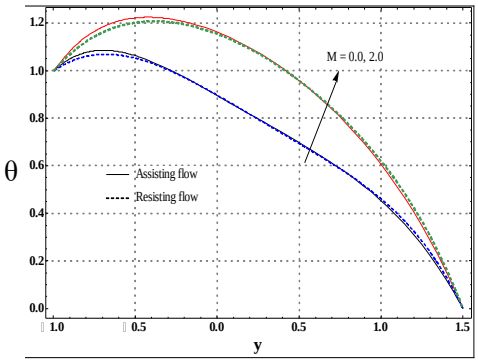

2 (d)

Figs. 1(a-e). Effects of various embedded parameters on the velocity profile.

Behavior of temperature is seen through Figs. 2 (a-f). Change in temperature is more dominant near the channel walls when compared with the center for assisting and opposing cases. It is clear that the temperature decreases by increasing B and β whereas it increases through increase in A, α, M and Du. Change in temperature corresponding to B and α is small. Also the temperature near the lower wall is less for opposing flow.

The concentration profile has been examined via Figs. 3 (a-e). Concentration at a particular part of the channel increases with increase in B but decreases with increase in A, Du, Sr and Sc. Decrease in concentration subject to an increase in A is less then corresponding increase in case of *Du*, *Sc* and *Sr*. Moreover, the concentration near the upper wall is higher when flow is assisting. Difference in concentration for assisting and opposing flows is enhanced by the variation in *Sr* and *Sc*.

Numerical values of the heat and mass transfer rates are given through the Tables 1 and 2 respectively. The values for assisting and opposing flows are given separately. Results showed that the heat transfer rate at the upper wall ($-\theta'(h_1)$) decreases by increasing B and β whereas it increases through A and M. Impact of B on the heat transfer rate is small when compared with the other parameters. Also the value of heat transfer rate is higher in case of opposing flow. Increase in the inclination angle α tends to increase the heat transfer rate in case of opposing flow whereas it decreases the transfer rate for assisting flow.

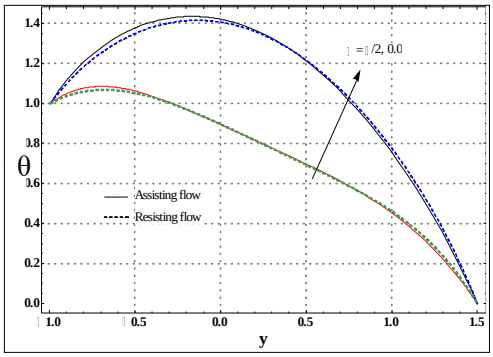

2 (e)

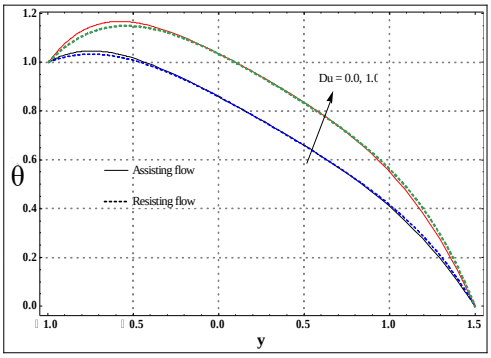

2 (f)

Figs. 2(a-f). Variation of temperature subject to change in the values of embedded parameters.

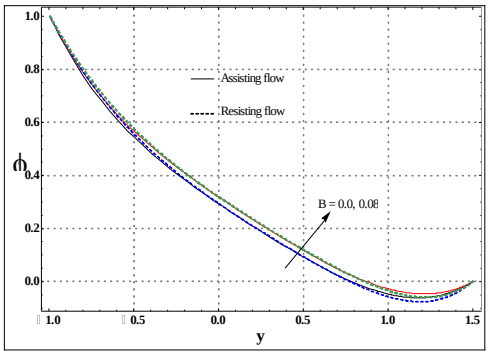

3 (a)

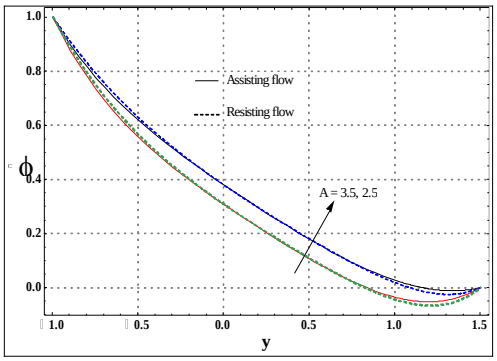

3 (b)

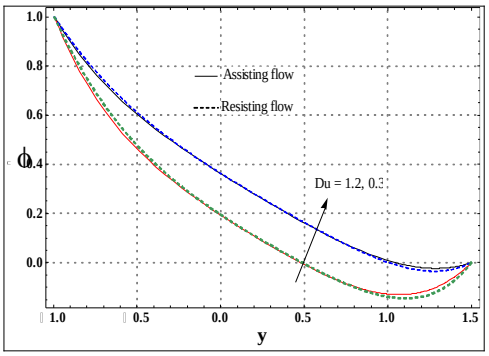

3 (c)

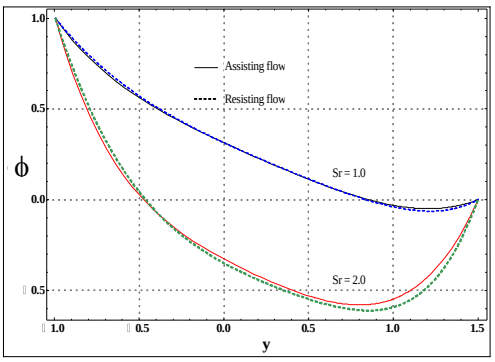

3 (d)

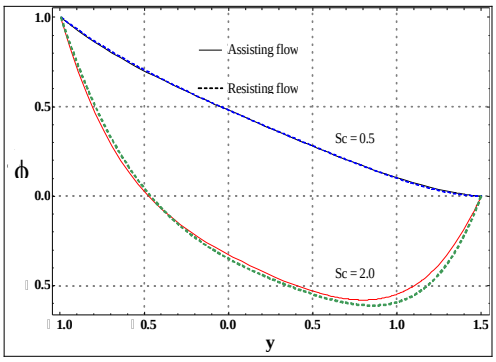

3 (e)

Figs. 3(a-e). Influence of pertinent parameters on the concentration.

Numerical values of mass transfer rate at the upper wall ($-\varphi'(h_1)$) are given in Table 2. The value of mass transfer rate at the upper wall is found to increase when B and β are increased. However it decreases for large A and M. When the channel inclination is increased from 0 to $\pi/2$ then the mass transfer rate increases for assisting flow and it decreases for opposing flow.

MAIN FINDINGS

This study examined the inclined magnetic field effects on the peristaltic flow in an inclined channel. Key findings of present study are summarized in following points

- Parabolic velocity profile tends to shift from center of the channel towards the channel walls

as we move from assisting to opposing flow.

- Velocity and temperature decrease whereas concentration increases by increasing B.
- The dependence of magnetic field on the angle is quite significant.
- Temperature and concentration fields in opposing flow are reverse.
- Effects of channel inclination on heat and mass transfer rates at the wall are opposite in the assisting and opposing flows

Table 2 Mass transfer rate at h_1 for assisting and opposing flows

B	A	M	β	α	Assisting flow	Opposing flow
0.0	3.5	1	$\frac{\pi}{4}$	$\frac{\pi}{2}$	0.1560	0.07644
0.08					0.1619	0.0818
0.05	2.5				0.2312	0.1506
	3.5				0.1597	0.0798
		0			0.1814	0.1032
		2			0.0943	−0.4641
		1	0		0.1379	0.0565
			$\frac{\pi}{2}$		0.1814	0.1032
			$\frac{\pi}{4}$	0	0.1252	0.1252
				$\frac{\pi}{2}$	0.1597	0.0798

REFERENCES

Abbasi, F. M., A. Alsaedi and T. Hayat (2014). Peristaltic transport of Eyring-Powell fluid in a curved channel *Journal of Aerospace* Engineering 27, 04014037.

Abbasi, F. M., T. Hayat and B. Ahmad (2015). Peristaltic transport of copper-water nanofluid saturating porous medium, Physica E: Low-dimensional *Systems and Nanostructures 67 (2015), 47-53.*

Abbasi, F. M., T. Hayat, B. Ahmad and G. Q. Chen (2014). Peristaltic motion of non-Newtonian nanofluid in an asymmetric channel. *Z. Naturforsch 69, 451-461*.

Abbasi, F. M., T. Hayat, B. Ahmad and G. Q. Chen (2014). Slip effects on mixed convective peristaltic transport of copper-water nanofluid in an inclined channel. *PLos ONE, Vol. 9(8), pp. e105440.*

Abbasi, F. M., T. Hayat, A. Alsaedi and B. Ahmed (2014). Soret and Dufour effects on peristaltic transport of MHD fluid with variable viscosity. Applied *Mathematics & Information Sciences 8, 211-219.*

Abd elmaboud, Y. and Kh. S. Mekheimer (2011). Non-linear peristaltic transport of a second-order fluid through a porous medium. *Applied Mathematical Modelling 35, 2695-2710*

Akbar, N. S., S. Nadeem and C. Lee (2013). Biomechanical analysis of Eyring Prandtl fluid model for blood flow in stenosed arteries. *International Journal of Nonlinear Sciences and Numerical Simulation 14, 345-353.*

Haya, T., F. M. Abbasi and S. Obaidat (2011). Peristaltic motion with Soret and Dufour effects. *Magnetohydrodynamics 47, 295-302.*

Hayat, T, F. M Abbasi, A. Alsaedi and F. Alsaadi (2014). Hall and Ohmic heating effects on the peristaltic transport of Carreau-Yasuda fluid in an asymmetric channel. *Z. Naturforsch 69, 43-51*.

Hayat, T., F. M. Abbasi and A. A. Hendi (2011). Heat transfer analysis for peristaltic mechanism in variable viscosity fluid. *Chinese Physics Letters 28, 044701*.

Hayat, T., F. M. Abbasi, B. Ahmad and A. Alsaedi (2014). MHD mixed convection peristaltic flow with variable viscosity and thermal conductivity. *Sains Malaysiana 43, 1583-1590.*

Hayat, T., F. M. Abbasi, B. Ahmad and A. Alsaedi (2014). Peristaltic transport of Carreau-Yasuda fluid in a curved channel with slip effects. *PLoS ONE 9(4), 95070.*

Hayat, T., F. M. Abbasi, M. S. Alhuthali, B. Ahmad and G. Q. Chen (2014). Soret and Dufour effects on peristaltic transport of a third order fluid. *Heat Transfer Research 45, 589-603.*

Kabir, K. H., M. A. Alim and L. S. Andallah (2015). Effects of stress work on MHD natural convection flow along a vertical wavy surface with Joule heating. *Journal of Applied Fluid Mechanics 8, 213-221.*

Kothandapani, M. and S. Srinivas (2008). On the influence of wall properties in the MHD peristaltic transport with heat transfer and porous medium. *Physics Letters A 372, 4586-4591*.

Lew, S. H., Y. C. Fung and C. B. Lowenstein (1971). Peristaltic carrying and mixing of chime. *Journal of Biomechanics 4, 297-315.*

Maiti S. and J. C. Misra (2011). Peristaltic flow of a fluid in a porous channel: A study having relevance to flow of bile within ducts in a pathological state. *International Journal of Engineering Science 49, 950-966.*

Pandey, S. K. and M. K. Chaube (2011). "Peristaltic flow of a micropolar fluid through a porous medium in the presence of an external magnetic field. *Communications in Nonlinear Science and Numerical Simulations 16, 3591-3601*.

Srinivas, S. and V. Pushparaj (2008). Non-linear peristaltic transport in an inclined asymmetric channel. *Communications in Nonlinear Science and Numerical Simulations 13, 1782-1795.*

Srivastava, L. M. and P. V. Srivastava (1988).

Peristaltic transport of a power law fluid: Applications to the ductus efferentes of the reproductive tract. *Rheology Acta 27, 428-433.*

Tripathi D. (2011). Peristaltic transport of a viscoelastic fluid in a channel. *Acta Astronautica 68, 1379-1385.*

Tripathi D., S. K. Pandey and S. Das (2011). Peristaltic transport of a generalized Burgers' fluid: Application to the movement of chyme in small intestine. *Acta Astronautica 69, 30-38*.

Variational methods for problems from plasticity theory and for generalized Newtonian fluids, Lecture Notes in Mathematics, Fluids of Prandtl-Eyring type and plastic materials with logarithmic hardening law. Springer (2007), 1749, 207-259.